

www.acsnano.org

Suppressing Efficiency Roll-Off at High Current Densities for Ultra-Bright Green Perovskite Light-Emitting Diodes

Chen Zou, Yun Liu, David S. Ginger, and Lih Y. Lin*



Cite This: ACS Nano 2020, 14, 6076-6086



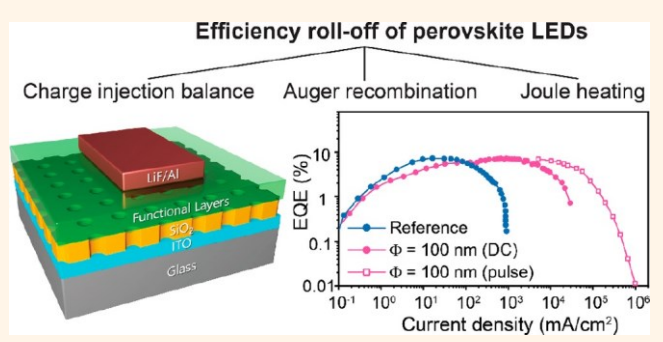
ACCESS I

Metrics & More

Article Recommendations

Supporting Information

ABSTRACT: Perovskite light-emitting diodes (PeLEDs) have undergone rapid development in the last several years with external quantum efficiencies (EQEs) reaching over 21%. However, most PeLEDs still suffer from severe efficiency rolloff (droop) at high injection current densities, thus limiting their achievable brightness and presenting a challenge to their use in laser diode applications. In this work, we show that the roll-off characteristics of PeLEDs are affected by a combination of charge injection imbalance, nonradiative Auger recombination, and Joule heating. To realize ultrabright and efficient PeLEDs, several strategies have been applied. First, we designed an energy ladder to balance the electron and hole transport.



Second, we optimized perovskite materials to possess reduced Auger recombination rates and improved carrier mobility. Third, we replaced glass substrates with sapphire substrates to better dissipate joule heat. Finally, by applying a currentfocusing architecture, we achieved PeLEDs with a record luminance of 7.6 Mcd/m². The devices can be operated at very high current densities (J) up to ~1 kA/cm². Our work suggests a broad application prospect of perovskite materials for highbrightness LEDs and ultimately a potential for solution-processed electrically pumped laser diodes.

KEYWORDS: perovskite light emitting diodes, efficiency roll-off, ultrahigh brightness, high injection current density, charge injection balance, Auger recombination, Joule heat

olution-processed metal hybrid perovskites exhibit excellent luminescence, high color purity, and tunable emission wavelengths, making them promising candidates for low-cost, high-performance light-emitting diodes (LEDs) and laser diodes (LDs). 1-15 Previously reported highefficiency PeLEDs are mainly based on quasi-2D perovskites with multiple quantum wells (MQWs) in an effort to provide confinement for electron-hole pairs and thus increase the photoluminescence quantum yield (PLQY). However, for most of these quasi-2D PeLEDs, the peak EQE is achieved at a very low current density ($J < 0.1 \text{ mA/cm}^2$) and starts to drop significantly at high J. 16 This detrimental behavior is described as efficiency roll-off, which is likely caused by a combination of charge injection imbalance, Auger-induced luminescence quenching, and Joule heating. 16-20 This efficiency roll-off, also known as droop, can be quantified by the critical current density (J_c) that corresponds to the value of J at which the EQE reduces to half of its peak value.²¹ For most reported green PeLEDs, J_c remains in the regime of 1-100 mA/cm², ^{2,6,8} limiting their achievable brightness to below 100 000 cd/m². A record luminance of 510 000 cd/m² with an EQE of 9.3% for

PeLEDs has been achieved only very recently by Sim et al., who replaced quasi-2D with 3D perovskites.²² However, this value is still lower than the record for quantum dot LEDs,²³ which is $614\,000\,\text{cd/m}^2$ for green emission.

Suppressing efficiency roll-off at high J is also a necessary step toward electrically pumped perovskite laser diodes (PeLDs), which could in principle be enabled by perovskites' low amplified spontaneous emission (ASE) thresholds and long carrier diffusion lengths.²⁴ However, one vital problem needs to be overcome, namely, how to inject high J of over several hundreds of A/cm² without significant exciton quenching.^{25,26} These high current densities are needed

Received: March 2, 2020 Accepted: April 23, 2020 Published: April 23, 2020





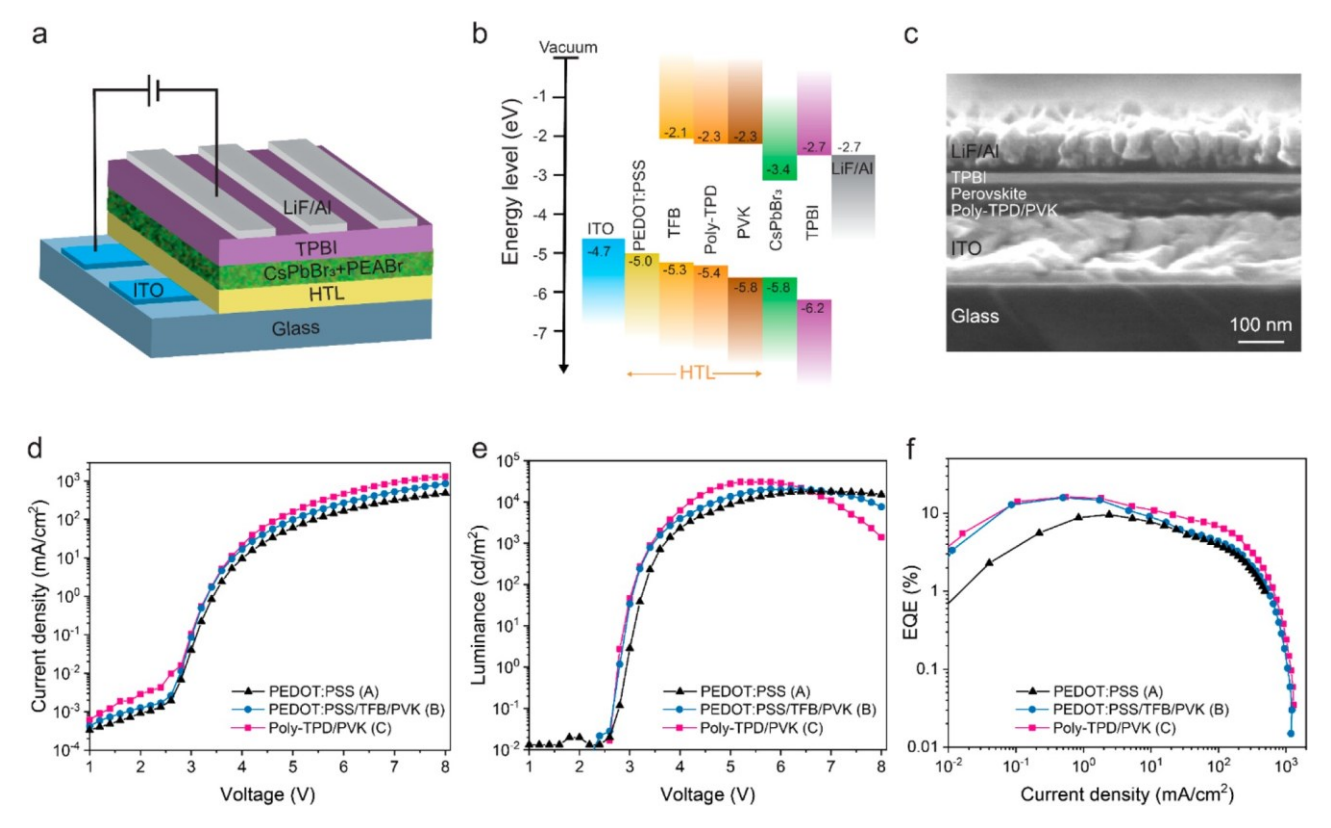


Figure 1. Performance comparison of quasi-2D PeLEDs based on different HTLs. (a) Schematic structure architecture. (b) Energy level diagram of quasi-2D PeLEDs with various HTLs. (c) High-resolution SEM cross-sectional image. (d) J–V, (e) L–V, and (f) EQE–J data of Structures A, B, and C.

because the key parameter of $J \times EQE$ or luminance (L) need to be large enough to exceed the lasing threshold.²⁶

Although eliminating efficiency roll-off is important to the development of both high-brightness LEDs and electrically pumped laser diodes for a variety of applications in lighting, projection display, and phototherapy, only a few studies on this topic have been reported for PeLEDs to date. 16,20,21,27-2 Herein, we demonstrate, in quasi-2D PeLEDs, suppression of efficiency roll-off by balancing charge injection via building an "energy ladder" in hole transport layers. Upon optimization, we achieved simultaneously high EQE (16.2%) and luminance (~31 000 cd/m²). Next, to increase carrier mobility and reduce nonradiative Auger recombination, we replaced the insulating long-chain spacer (PEABr) in the quasi-2D perovskite with small cation KBr. The resulting luminance improves by about 4-fold to $\sim 120~000~\text{cd/m}^2$, and J_c increases by 20-fold to ~800 mA/cm². Subsequently, we investigated thermalinduced luminescence quenching by comparing glass and sapphire substrate based PeLEDs and show that Joule heat produced during device operation significantly affects the rolloff characteristics. 19 To further mitigate Joule heating, we fabricated current-focusing devices with small current injection areas and operated them under pulsed current injection. The generated Joule heating can be dissipated to the surrounding insulator area, thus improving heat sinking capability. Pulsed current operation helps devices survive at higher J by further reducing the average heating rate. Together, these strategies allow us to increase J_c up to $\sim 60 \text{ A/cm}^2$ (54-fold improvement compared to the best previously reported values²¹) while operating the device at J values up to $\sim 1 \text{ KA/cm}^2$ (highest reported among PeLEDs) without measurable damage to

either the perovskite or injection layers, ultimately leading to a record luminance of 7.6 Mcd/m².

RESULTS AND DISCUSSION

Reducing the Efficiency Roll-Off by Balancing Charge Injection. For many noninverted PeLEDs, there is no energy barrier for electron injection between common electron transport layers (ETLs) like 2′,2′-(1,3,5-benzinetriyl)-tris(1-phenyl-1-H-benzimidazole) (TPBi) and perovskite layers. However, hole injection is not efficient due to the energy barrier between common hole transport layers (HTLs) and perovskite layers. ^{30,31} As a result, electron and hole charge injection are often not balanced, resulting in deterioration of PeLED performance. In addition, the electron—hole pairs tend to be quenched near the interface between the HTL and perovskite layer due to the unmatched energy levels, which causes nonnegligible luminescence quenching, especially for green- and blue-emitting PeLEDs. ^{32,33}

We used the quasi-2D perovskite (PEABr)_xCsPbBr₃ (where x is the molar ratio of PEABr to CsPbBr₃) in our work first due to the enhanced PLQY originated from MQW confinement.³⁴ We fabricated quasi-2D PeLEDs with the device structure of ITO/HTL/Perovskite/TPBi/LiF/Al as schematically illustrated in Figure 1a. Different HTLs were adopted to improve hole injection, and the common HTL of PEDOT:PSS was used for comparison (Structure A). By inserting additional HTLs of TFB and PVK between the PEDOT:PSS and perovskite, a stepwise "energy ladder" is realized (Structure B). In addition, the bilayer HTL of poly-TPD/PVK was also used as an energy ladder (Structure C). Figure 1b shows the energy band diagram of these PeLEDs including various HTLs; the

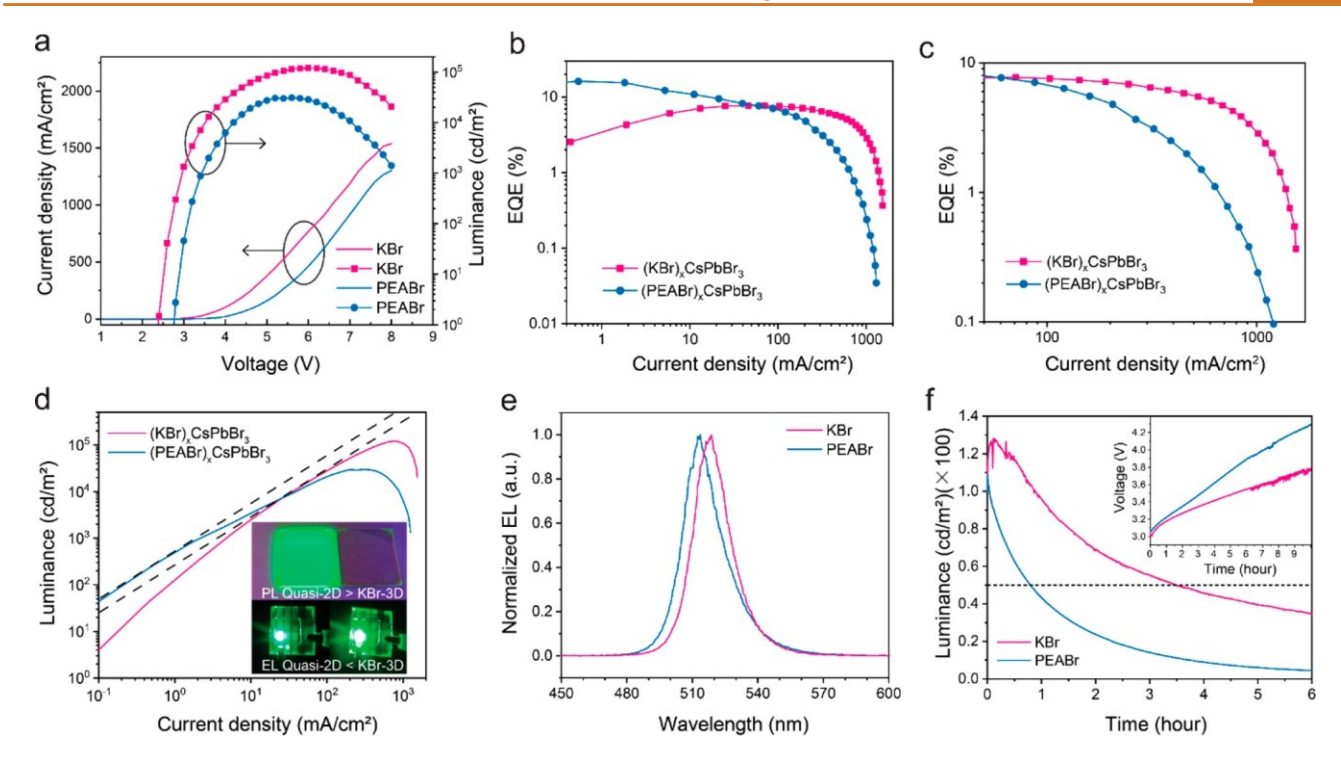


Figure 2. Performance comparison of PEABr- and KBr-based PeLEDs using the bilayer HTL of poly-TPD/PVK. (a) L-J-V data. (b) EQE versus J. (c) Efficiency roll-off comparison in the high J region (50 to 1500 mA/cm²). (d) L-J characteristics; the dashed lines indicate L-J curves without efficiency roll-off. The inset shows the real photos of PL and EL from PEABr- and KBr-based perovskite films. (e) EL spectra of PEABr- and KBr-based devices. (f) Luminance degradation with time; the initial luminance is 100 cd/m² for both devices. The inset shows the evolution of applied voltage during operation.

highest occupied molecular orbital (HOMO) energy level of CsPbBr₃ is -5.8 eV, while it is only ~-5.0 eV for PEDOT:PSS. Thus, a large energy barrier exists for hole injection from the PEDOT:PSS and perovskite layer, leading to inefficient hole injection and luminescence quenching at the interface. In contrast, the HOMO energy level of PVK is -5.8 eV, which is well-matched to the valence band edge of CsPbBr₃. The HOMO energy levels of TFB and poly-TPD are -5.3 and -5.4 eV, respectively, right between those of PEDOT:PSS and PVK. Figure 1c shows the cross-section view of Structure C obtained via scanning electron microscopy (SEM). Multiple layers are clearly visible in the following order (from bottom to top): ITO (~150 nm), poly-TPD/PVK(~35 nm), perovskite (~40 nm), TPBi (~40 nm), and LiF/A1(~70 nm).

We measured the current density-voltage (J-V) characteristics of all device structures (Figure 1d) and found Structure C showed the highest J whereas Structure A showed the smallest J. To further quantify charge injection, we measured the J-V characteristics of hole-only devices (based on different HTLs) and electron-only devices (Figure S1 in Supporting Information). The hole-only devices based on poly-TPD/PVK show the highest J compared to those of other devices based on PEDOT:PSS and PEDOT:PSS/TFB/PVK. These results confirm the poly-TPD/PVK HTL best enhances the hole injection efficiency and improves the number of injected holes. Furthermore, we found that electrons dominate charge injection into quasi-2D perovskite devices, and a more balanced charge injection occurs in the case of poly-TPD/ PVK devices. The perovskite films formed on different HTLs all exhibit smooth and continuous surface morphologies without obvious pinholes (See details in Figure S2 and S3).

The leakage J for Structure A, B and C is at a low level below 10⁻³ mA/cm², confirming good coverage of perovskite films on different HTLs used here. We further compare the luminancevoltage (L-V) characteristics (Figure 1e), the turn on voltage (defined as the voltage at which the luminance is 1 cd/m²) of multilayer HTL devices (Structures B and C, ~2.8 V) is also lower than that for the single layer HTL device (Structure A, ~ 3 V), consistent with the reduced energy barrier and enhanced hole injection through the energy ladder. Table S1 (Supporting Information) summarizes the performance parameters of Structures A, B, and C. Structure A shows a maximum luminance of 18154 cd/m², which is further increased to 20 342 and 31 012 cd/m² for Structures B and C, respectively. The 1.7-fold brightness improvement from Structure A to Structure C has been achieved through improving the hole injection efficiency and balancing charge injection.

The maximum EQEs for Structures A, B, and C are 9.6%, 15.8%, and 16.2%, respectively (Figure 1f). Structure C exhibits the best efficiency roll-off suppression performance with an EQE higher than Structures A and B in a wide range of J from 0.01 to 1000 mA/cm². We also observe that the devices with multilayer HTLs (Structures B and C) show higher EQEs compared to the single-layer HTL device (Structure A). We propose this result is due to either of two causes: (1) suppressed luminescence quenching at the interface between the HTL and the perovskite layer or (2) more balanced charge injection originated from improved hole injection efficiency. 32,35 We note that Structure C shows a similar EQE to Structure B at low J (0.01–10 mA/cm²). However, the EQE of Structure B drops faster after ~10 mA/cm², which indicates the imbalanced charge injection at high J for Structure B. This

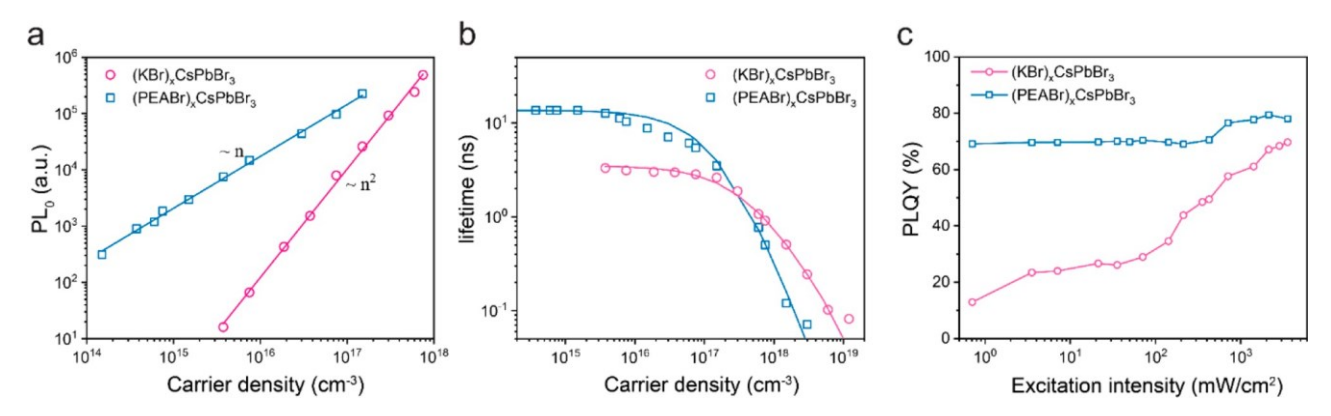


Figure 3. Investigation of carrier recombination dynamics of PEABr- and KBr-based perovskite films. (a) Dependence of PL_0 and (b) lifetime ($\tau_{1/e}$) on carrier density (n). (c) Internal PLQY as a function of incident excitation intensity.

finding is consistent with Figure 1d, where Structures B and C have almost the same J at low voltage (2.8–3.8 V) and start to show larger discrepancy at high voltage (after 3.8 V, 10 mA/cm²).

Although the efficiency roll-off of quasi-2D PeLEDs can be suppressed by reducing charge injection barriers, typical quasi-2D PeLEDs still suffer from severe efficiency roll-off at high J, likely due to the poor charge transport with the insulating long-chain PEABr layer and increased nonradiative Auger recombination rate originated from the enhanced local charge carrier density in the MQW structures (Figure S4). 20,36 The quasi-2D PeLEDs (x = 0.4) achieve much higher peak EQE than the 3D counterparts (x = 0); however, they show similar or even worse performance at high J (Figure S5). These characteristics hinder quasi-2D PeLEDs from maintaining high efficiency at high J and achieving ultrahigh brightness, motivating us to further contrast the performance of quasi-2D and 3D perovskites.

Higher Brightness and Enhanced Stability from KBr-Treated 3D Perovskite LEDs. For the practical applications of LEDs and the development of electrically pumped laser diodes, a key parameter of devices is the J × EQE (or brightness). 3D perovskites generally can withstand higher J; however, their PLQY is usually lower due to small exciton binding energy. ^{37–39} However, high PLQYs are achievable with proper surface passivation of 3D perovskites. ^{40–42}

Recently, Abdi-Jalebi et al. reported the enhanced luminescence from 3D perovskites following potassium passivation. ⁴² Following this method, we introduced excess KBr during CsPbBr₃ synthesis to form KBr-treated 3D perovskites. Enhanced photoluminescence (PL) was also observed for these KBr-treated 3D perovskite films (Figure S6). The device structure of the KBr treated PeLEDs studied here is the same as Structure C of the quasi-2D PeLEDs described above.

The KBr-based PeLEDs show higher J compared to PEABr-based counterparts (Figure 2a), which indicates the higher conductivity of KBr-based perovskite films as the additive KBr distrupts the 3D perovskite conduction much less than the incorporation of the large insulating cation of PEABr (and the formation of quasi-2D layers). The KBr-based PeLEDs also show a lower turn-on voltage of 2.4 V, which is the same as the bandgap of CsPbBr₃, consistent with barrier-free injection of charge carriers. In addition, compared to the PEABr-based devices, the KBr-based PeLEDs exhibit a suppressed luminance droop and approximately 4-fold luminance enhancement.

The KBr-based PeLEDs show smaller EOEs in the low J region, but then they exceed that of quasi-2D PeLEDs when J $> \sim 50 \text{ mA/cm}^2$ (Figure 2b). Although the peak EQE of the KBr-based PeLEDs (7.7%) is lower than that of the quasi-2D counterparts (16.2%), we highlight that the KBr-based PeLEDs exhibit suppressed efficiency roll-off, allowing better performance at high drive current densities (Figure 2c). The EQE for the KBr-based LEDs at a high J of 1000 mA/cm² remains at \sim 3%, which is a 10-fold enhancement compared to the PEABrbased PeLEDs at such a high J. In Figure 2d, the black dashed lines represent simulated L-J curves that might be expected without efficiency roll-off. The L-J curve of the KBr-based PeLEDs overlaps more with the ideal curve. The maximum luminances for KBr- and PEABr-based PeLEDs are 120 187 and 31 012 cd/m² with the corresponding J_c of ~800 and 40 mA/cm², respectively. The detailed performance comparison is included in Table S2. It should be noted the PL intensity of the KBr-based 3D perovskites is much smaller than that of PEABrbased quasi-2D perovskites under the excitation from the UV lamp (inset photograph of Figure 2d); however, the electroluminescence (EL) is 4-fold enhanced, suggesting even higher performance could possibly be achieved with higher-quality 3D perovskite samples. We will discuss these phenomena in more detail later.

The EL spectrum of KBr-treated 3D PeLEDs shows a narrow fwhm of 19 nm with the peak wavelength located at 519 nm (Figure 2e), which is slightly red-shifted in contrast to that of quasi-2D PeLEDs (513 nm, fwhm 20 nm). The higher bandgap of quasi-2D perovskite is due to the formation of MQWs. Operational stability is an important parameter for evaluating PeLEDs; ^{43–45} we measured the evolution of luminance with time for both devices (Figure 2f). The initial luminance was kept at 100 cd/m², and the J was kept constant. It is clearly observed that the KBr-based PeLEDs show much slower luminance decay compared to the PEABr-based PeLEDs. We introduce a key parameter T₅₀ to quantitatively compare the operation stability of both devices, which is defined as the time it takes for the luminance to decrease to half of its initial value. The T₅₀ values for PEABr- and KBrbased PeLEDs are 0.8 and 3 h, respectively, showing better operation stability of KBr-based PeLEDs. The inset figure shows that the applied voltage of both devices increases steadily with time to maintain a constant J. However, KBrbased PeLEDs show a slower voltage increase, which may be of help to suppress the ion migration across devices due to the reduced electric field.

Table 1. Fitted Recombination Coefficients from Transient PL Decay Measurement for Perovskite Films of Different Compositions

film	\mathbf{k}_1 (\mathbf{s}^{-1})	$k_2 (cm^3 s^{-1})$	$k_3 (cm^6 s^{-1})$
$(PEABr)_x(CsPbBr_3)$	7.3×10^7 (excitonic)	$(1.7 \pm 0.3) \times 10^{-9}$	$(6.5 \pm 0.8) \times 10^{-27}$
$(KBr)_x(CsPbBr_3)$	2.9×10^8 (trap assisted and radiative pseudo-first order recombination)	$(2.0 \pm 0.1) \times 10^{-9}$	$(2.9 \pm 0.4) \times 10^{-28}$

Carrier Recombination Dynamics of PEABr and KBr-Based Perovskite Thin Films. The charge carrier dynamics can be described with the following equation 46,4

$$\frac{\mathrm{d}n(t)}{\mathrm{d}t} = G - k_1 n - k_2 n^2 - k_3 n^3 \tag{1}$$

where n is the charge carrier density, t is the time, G is the generation rate, k₁ is the monomolecular recombination rate, k₂ is the bimolecular recombination rate, and k₃ is the Auger recombination rate. In general, the monomolecular recombination can be divided into trap-assisted recombination, excitonic recombination, and pseudo-first order recombination of minority carriers at low injection levels. The former is nonradiative while the latter two can be radiative.³⁸ Bimolecular recombination is a radiative process which emits photons, while Auger recombination is a nonradiative process which involves three or more charge carriers and converts energy to phonons.4

To analyze the different performances of PEABr- and KBrbased PeLEDs, we recorded the transient PL decays of both perovskite thin films under femtosecond pulsed excitation (λ = 365 nm). Figure 3a summarizes the PL_0 (the initial PL intensity, emitted in coincidence with the excitation laser pulse) as a function of carrier density for both samples. For the KBr-based perovskites, the quadratic power dependence of the PL₀ on the carrier density is consistent with radiative bimolecular recombination in competition with monomolecular nonradiative recombination. In contrast, for the PEABrbased perovskites, PL₀ increases linearly with the carrier density, indicating that PL originates from monomolecular recombination of bound excitons. This result is consistent with the formation of MQWs which provides confinement for the photoexcited geminate electron-hole pairs and thus increases the exciton binding energy.

The dependence of the effective lifetime $(\tau_{1/e})$ as a function of the carrier density for PEABr- and KBr-based perovskites is shown in Figure 3b. Such dependence can be well-fitted by eq 1, following the method proposed by Xing et al.³⁷ The fitted recombination coefficients are presented in Table 1, which are consistent with previous reports. 5,38,46 Although the monomolecular recombination is mainly nonradiative in KBr-based perovskites, the k₂ value of KBr-based perovskites is slightly higher than that of PEABr-based perovskites, ensuring that the KBr-based perovskites can achieve comparably high PLQY as PEABr-based perovskites. In addition, it should be noted that k3 for KBr-based perovskites is one order smaller than that of PEABr-based perovskites, indicating suppressed Auger recombination in KBr-based perovskites.

Figure 3c presents the internal PLOY of our PEABr- and KBr-based perovskite films measured under different continuous wave (CW) laser excitation intensities. The internal PLQY was calculated based on the light escape probability and measured external PLQY by a model accounting for photon recycling and the light outcoupling effect (see details in Supplementary note 1, Supporting Information).^{39,42} The PEABr-based perovskite films show a nearly invariant internal

PLQY as high as 70% at excitation intensities below 500 mW/ cm², which is attributed to the first-order excitonic emission under low excitation density conditions. Under LED working conditions, where the carrier density is typically <10¹⁵ cm⁻³ (corresponding to ${\sim}600\,\text{mW/cm}^2$), the nearly invariant high PLQY at low carrier density for PEABr-based perovskite films ensures the high EQE of quasi-2D PeLEDs at low injected J. Above 500 mW/cm², The PLQY slightly increases as the radiative bimolecular recombination becomes effective. Unfortunately, we could not further increase the excitation intensity due to the limitation of maximum power provided by our CW laser. Therefore, the expected behavior that PLQY declines at a higher excitation intensity was not observed. For KBr-based perovskite films, the PLQY starts at a relatively low value under low excitation intensity, which is consistent with high levels of nonradiative recombination in KBr-based perovskites. However, the PLOY increases significantly when the excitation intensity is above 100 mW/cm² as the radiative recombination from free electron-hole pairs starts to dominate. This observation clearly reveals that the EQE limitation for KBr-based PeLEDs at a relatively low current density is from the nonradiative recombination losses, likely due to defect-mediated recombination. However, at the high excitation intensity region, the PLQY of KBr-based perovskite films is close to that of the PEABr-based perovskite films. Therefore, defect passivation is likely desired to further improve the peak EQE of KBr-based 3D PeLEDs.

Under steady-state excitation, the PLQY $(\eta(n))$ for 3D perovskites is given by³⁸

$$\eta(n) = \frac{k_r + k_2 n}{k_1 + k_2 n + k_3 n^2} \tag{2}$$

where k_r is the radiative "pseudo-monomolecular" decay coefficient due to the recombination of minority photoexcited carriers with intrinsic majority carriers at low fluence. The PLQY should be strongly dependent on n. It first increases with increasing n as the radiative biomolecular recombination gradually dominates over the nonradiative trap-assisted monomolecular recombination. At high carrier density, where the three-body Auger recombination becomes effective and dominates over the bimolecular recombination, the PLQY will in turn decrease with increasing n. In order to study the effect of the individual rate constant on PLQY, we calculated carrier density dependent PLQY with two recombination coefficients fixed and one varied at some typical values (Figure S7). We found that a high-quality 3D perovskite film requires small k₁ and k₃ and large k₂. Furthermore, for the purpose of suppressing the PLQY droop at high carrier density and enhancing the luminance of PeLEDs, only small k₃ and large k₂ are particularly required as k₁ almost only affects the PLQY at low carrier density. Since KBr-treated 3D perovskites show lower Auger recombination, we conclude that 3D perovskites are better suited for suppressing efficiency roll-off, and the PeLEDs in the next parts of this work are all based on KBrtreated 3D perovskites.

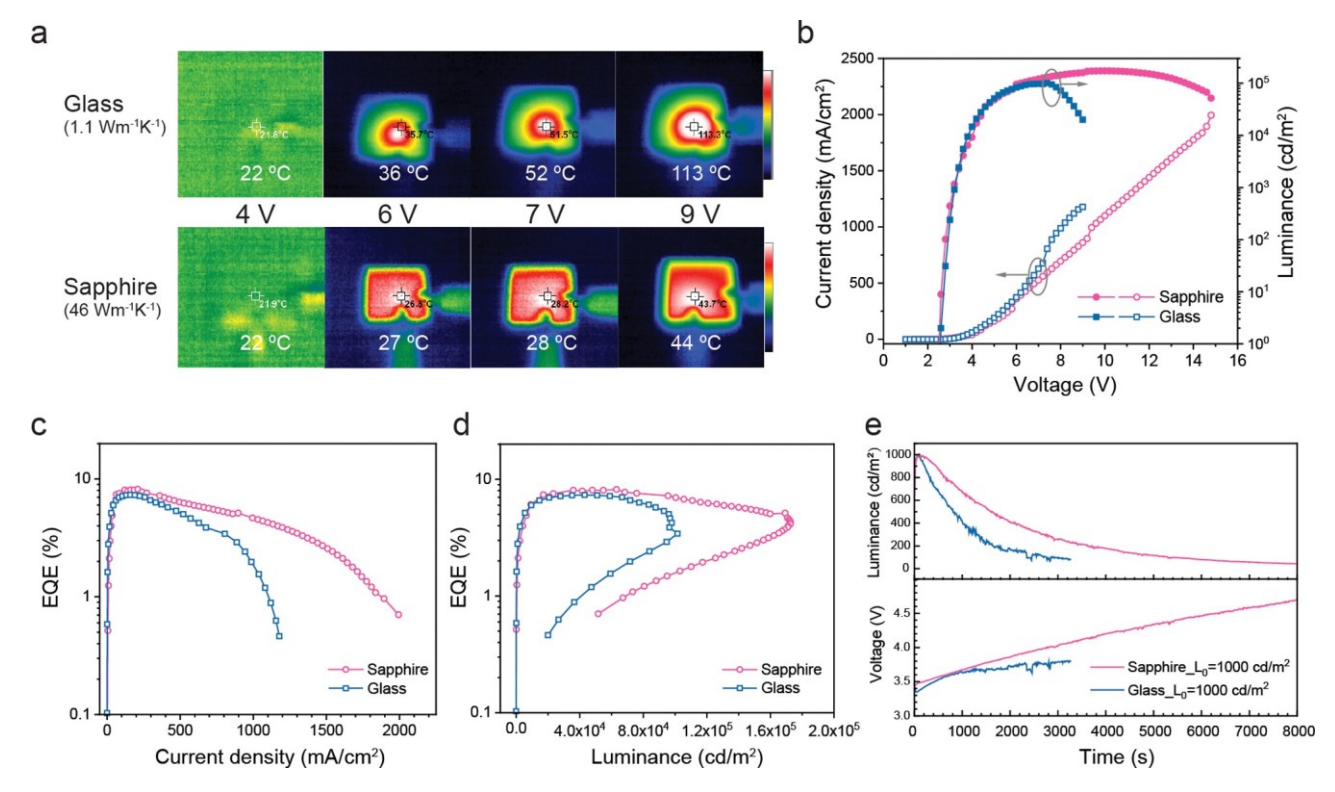


Figure 4. Replacing glass with sapphire substrates to reduce thermal-induced efficiency roll-off. (a) Surface temperature distributions of KBr-based PeLEDs based on glass and sapphire substrates at various voltages. (b) L-J-V, (c) EQE-J, and (d) EQE-L characteristics of glass-and sapphire-based devices. (e) Evolution of luminance and voltage for both devices; the initial luminance is 1000 cd/m^2 .

Thermal Management through Sapphire Substrates with Higher Thermal Conductivity. Another critical factor that contributes to the efficiency roll-off is Joule heating. At high J, due to the presence of leakage current and nonradiative Auger recombination, a large amount of energy is released in the form of heat, leading to the increase of device temperature. The generation of joule heat could cause crystal distortions, surface traps, and ion migration, thus deteriorating the PLQY and other optoelectronic properties of perovskite films. In addition, perovskite materials usually have poor thermal stability, and devices could break down or even burn out at elevated temperatures.

To assess local heating, we measured the substrate temperature distributions of glass- and sapphire-based PeLEDs at various drive voltages using an infrared camera (Figure 4a). The temperature images were all captured after applying a specific voltage for 30 s. The glass substrate temperature rises rapidly with increasing voltage, reaching up to 113 °C at 9 V. It should be noted that the temperature of the LED junction could be even higher than the observed surface temperature due to the low thermal conductivity of functional layers in PeLEDs. At such a high temperature, the perovskite active layer, as well as the injection layers, could be damaged or destroyed. We proposed that, by using transparent sapphire substrates as heat sinks, the Joule heating could be more effectively dissipated as sapphire has a much higher thermal conductivity (46 W m⁻¹ K⁻¹) compared to glass (1.1 W m⁻¹ K⁻¹). Figure 4a confirms this hypothesis, with the substrate temperature of sapphire-based PeLEDs increasing only moderately from 22 °C at 4 V to only 44 °C at 9 V. We also note that the temperature distribution of the sapphire substrate is more uniform compared to the glass substrate, meaning that Joule heat can efficiently diffuse into the

surroundings through the whole sapphire substrate as a result of the higher thermal conductivity.

As the emission properties of perovskite materials are significantly affected by temperature, 48 the better thermal dissipation of sapphire substrates should both help PeLEDs survive at a higher J and suppress thermal-induced efficiency roll-off. To confirm this hypothesis, we compare the L-J-V characteristics of PeLEDs on glass and sapphire substrates (Figure 4b). Both devices exhibit similar J-V characteristics at low voltage (<7 V). Nevertheless, the glass-based devices show a larger J than that of sapphire-based devices at higher voltage. This is because Joule heating can accelerate the hopping of charge carriers in perovskite materials, thus speeding up charge carrier injection and transport. For L-V characteristics, both devices exhibit a similar luminance rise with increasing voltage at the beginning (<7 V). However, the luminance of glassbased devices shows a faster decline after 7 V. In contrast, sapphire-based devices are able to maintain a high luminance value with minor drop-off up to 15 V. Almost no EL can be detected from glass-based substrates at such a high voltage due to damage to perovskite layers.

Figure 4c shows EQE-J characteristics for PeLEDs on glass and sapphire substrates. It is clearly observed that efficiency roll-off is significantly suppressed for PeLEDs on sapphire substrates. The EQE for sapphire-based devices still maintains a high value of 2.6% at a high J of 1.5 A/cm². It should be also noted that sapphire-based devices achieve a higher peak EQE (8.2%) compared to glass-based ones (7.3%), which is attributed to higher light outcoupling efficiency of the former (see optical simulations of light outcoupling from PeLEDs in Supplementary note 2 and Figure S8).⁴⁹ A more distinct comparison of efficiency roll-off can be acquired from the EQE-L characteristics (Figure 4d). The EQE of sapphire-

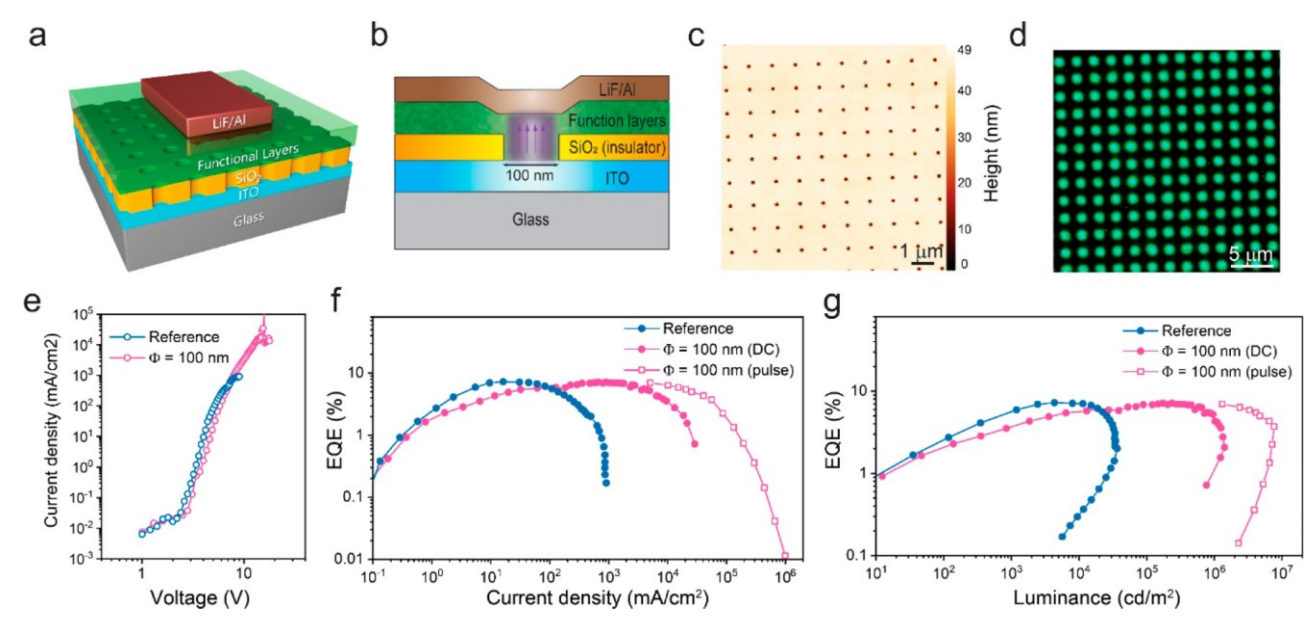


Figure 5. Suppressing Joule heating by nanopatterning the current injection area. (a) Schematic device structure with nanodot-shaped current apertures in the SiO_2 (insulator) layer. (b) Schematic illustration of current flowing in nanopatterned PeLEDs. The functional layers include HTL, KBr-based perovskite, and TPBi. (c) AFM image of the SiO_2 layer. (d) Dark-field optical microscope image of nanopatterned PeLEDs ($\Phi = 1 \mu m$) under operation at 10 V, showing EL only from patterned current apertures. (e) J–V data for reference and nanopatterned PeLEDs ($\Phi = 100 \text{ nm}$). (f) EQE–J and (g) EQE–L characteristics for reference, nanopatterned PeLEDs in DC and pulsed current (pulse duration 2 μ s, duty cycle 0.2%).

based devices exhibits a milder decline with increasing luminance in contrast to the glass-based ones. Both devices show a cliff-like efficiency droop where the luminance achieves the maximum value and starts to decrease, which indicates both devices go through the destruction of the functional layers after applying a sufficiently large voltage or current density. However, the maximum luminance of sapphire-based devices is ~1.7-fold higher than that of glass-based devices, demonstrating better heat dissipation by using sapphire substrates

We also compare the operation stability of PeLEDs on glass and sapphire substrates with a high initial luminance of 1000 cd/m² (Figure 4e). The sapphire-based devices show slower luminance decay. The T_{50} lifetimes are 13 and 20 min for glass-and sapphire-based devices, respectively. The applied voltage of both devices goes up with time to maintain the constant J. For sapphire-based devices, the applied voltage increases from 3.7 to 4.6 V after about 2 h of operation. However, the applied voltage of glass-based devices seems to become steady after \sim 20 min, indicating possible device failures.

Applying the Current-Focusing Architecture and Pulsed Current Operation. In addition to using sapphire substrates for thermal management, we also apply a small-area current aperture strategy to help mitigate Joule heating. This strategy is effective because the generated Joule heat can diffuse from the current flow regions to the surrounding insulating layer which acts as a heat sink, thus improving the performance of PeLEDs at high J. Devices were also driven by pulsed current to further minimize the impact of Joule heating and ion migration. The suppressed efficiency roll-off was first successfully demonstrated by managing joule heating using a microsize current aperture structure ($\Phi = 200 \, \mu \text{m}$) (Figure S9). These devices show the highest J × EQE (0.41 A/cm²) and luminance (1.5 Mcd/m²) under pulsed current operation (pulse width 2 μs , duty cycle 0.2%), a 22-

fold enhancement from reference devices. Besides, J_c is improved to 7 A/cm², much higher than that of reference devices (0.8 A/cm²) (Table S3). It is interesting to note that the EL response time for KBr-based devices is much shorter than that of PEABr-based devices under pulsed current operation (pulse width 2 μ s), consistent the improved carrier mobility for KBr-treated 3D perovskite films (Figure S10).

To further mitigate Joule heating, we downsized the diameter of our current apertures to hundreds of nanometers. Figure 5a schematically illustrates the architecture of PeLEDs with the nanopatterned injection area. A 60 nm-thick SiO₂ was deposited on an ITO electrode as an insulator layer, and a small circular hole ($\Phi = 100 \text{ nm}$) was defined by electronbeam lithography. HTL, perovskite, ETL and electrode layers are subsequently deposited onto the substrate. The current flows are confined in these nanodot-shaped current apertures, as schematically shown in Figure 5b. To allow the emission to be detected by a photodetector, we fabricated an array of nanodots instead of a single nanodot in the insulator layer. The atomic force microscope (AFM) image presents the surface morphology of the insulator layer, demonstrating the uniformity of the nanodot array ($\Phi = 100 \text{ nm}$) (Figure 5c). We also inspected the EL emission from nanopatterned PeLEDs ($\Phi = 1 \mu m$) operated at 10 V by an optical microscope in dark field (Figure 5d). No EL was observed in the insulating regions, demonstrating that current flow regions are successfully constrained inside the apertures. We enlarged the current apertures here due to the diffraction limit of the optical microscope, which makes the EL emission from 100 nm-diameter apertures not observable. The J-V characteristics of nanopatterned and reference PeLEDs measured in DC mode are shown in Figure 5e. The reference devices show a maximum J (J_{max}) of ~1 A/cm² and voltage of ~9 V before device breakdown. In contrast, no obvious breakdown is observed in nanopatterned PeLEDs ($\Phi = 100 \text{ nm}$) until 15 V,

and J_{max} could be as high as 28.9 A/cm². The EQE-J and EQE-L characteristics (Figure 5f,g) clearly show efficiency roll-off is significantly suppressed for nanopatterned PeLEDs, especially operated in pulsed current mode. The nanopatterned PeLEDs driven by pulsed current achieve J_{max} up to $\sim 1~\text{KA/cm}^2$ without device failure. The maximum luminance of 7.6 Mcd/m² (corresponding to a J × EQE of 2.1 A/cm²) is obtained at J of \sim 56 A/cm², which, to the best of our knowledge, is a record luminance among PeLEDs. Besides, J_c is improved to 60 A/cm², a 75-fold enhancement from reference devices. More detailed characteristics are included in Table S3, and the performance comparisons between our devices in this work and other representative green-emission PeLEDs are summarized in Table S4. Further optimization of device performance should be achievable by adding the DC bias to the pulse train following the method proposed by Kim et al.²⁸ We attribute the improved performance from KBrtreated 3D nanopatterned PeLEDs mainly to significantly mitigated Joule heating. However, in theory, this structure can further be used to reduce exciton-polaron annihilation for materials whose charge carrier recombination is dominated by bound excitons. When the current aperture size is close to exciton diffusion length, some excitons can diffuse outside the nanodot-shaped apertures and escape from current flow regions where charge carriers move directionally under electric field, thus suppressing the exciton-polaron interactions. 53,54

Our KBr-based perovskite films exhibit an ASE threshold of $\sim 15 \, \mu \text{J/cm}^2$ (Figure S11). Based on the extracted k_1 , k_2 , and k_3 , we calculate that a J × EQE value of 95 A/cm² and a luminance of 350 M cd/m² are needed to realize electrically pumped lasing (Supplementary note 3 and Figure S12). Currently, the best J × EQE and luminance achieved here are still one order below the calculated lasing threshold. However, incorporation of resonance cavities such as distributed feedback (DFB) structures are likely to reduce the lasing threshold, and as such, we believe the electrically pumped PeLDs should be within reach. ^{13,15} At the same time, more work should be continued to optimize perovskite materials, heat management, pulse train operation, and long-term stability.

CONCLUSION

In summary, we have applied several strategies to suppress efficiency roll-off and improve brightness of PeLEDs. From the aspect of device engineering, we have designed an energy ladder to balance electron and hole injection. In terms of perovskite materials, we replaced quasi-2D perovskites by a KBr-treated 3D CsPbBr₃ perovskite due to its lower Auger coefficient. From the aspect of heat management, we observed that Joule heating is a key factor leading to efficiency roll-off at high J, both by thermal imaging and by comparing the performance of glass- and sapphire-based devices. To further suppress the Joule heating of PeLEDs, we applied a currentfocusing architecture with micro- and nanosize current apertures. The nanopatterned PeLEDs show a record luminance of 7.6 Mcd/m²; furthermore, the devices can be operated at a high J up to 1 KA/cm². Our work provides a route to achieve efficient, high-brightness PeLEDs with low efficiency roll-off. It also demonstrates the potential of perovskites for realizing solution-processed laser diodes with further optimization of the materials and devices.

EXPERIMENTAL SECTION

Materials. PbBr₂ (99.9%, metal basis), CsBr (99.9, metal basis), KBr (99.9%, metal basis), PEABr (98%), PVK (MW 25 000–50 000), and dimethyl sulfoxide (DMSO, anhydrous) were purchased from Sigma-Aldrich. Poly-TPD and TFB were purchased from American Dye Source. Chlorobenzene (anhydrous, 99.8%) and 1,4,7,10,13,16-hexaoxacyclooctadecane (18-crown-6, crown) (99%) were purchased from Acros. Poly(3,4-ethylenedioxythiophene) polystyrenesulfonate (PEDOT:PSS, AI 4083) and 2',2'-(1,3,5-benzinetriyl)-tris(1-phenyl-1-H-benzimidazole) (TPBi, 98%) was purchased from Ossila. All chemicals were used as received without further purification.

Preparation of Perovskite Films. The quasi-2D precursor solution was obtained by mixing 0.2 M CsBr and 0.2 M PbBr₂ with different amounts of PEABr and crown in DMSO at 60 °C for 2 h with constant stirring. The best molar ratio of PEABr to CsPbBr₃ is x = 40%. The KBr-treated 3D precursor solution was obtained by mixing 0.024 M KBr, 0.216 M CsBr, 0.2 M PbBr₂, and crown in DMSO at 60 °C for 2 h with constant stirring. The perovskite precursor solutions were spin-coated onto substrates at 3000 rpm for 60 s with an acceleration speed of 1500 rpm/s. Afterward, the perovskite films were immediately annealed at 100 °C for 1 min to accelerate nucleation. Unless specified, the concentration of crown is 3.5 mg/mL in perovskite precursor solutions.

LED Fabrication. All precursor solutions were filtered by $0.45~\mu m$ Nylon or PTFE syringe filters before use. The prepatterned ITO substrates (sheet resistivity 15 Ω /sq) were cleaned by critical cleaning detergent (Ossilla) in hot water with sonication for 5 min and then rinsed in DI water. The substrates were further cleaned in acetone, isopropyl alcohol, and deionized water with sonication for 5 min in sequence. The cleaned substrates were dried by an air gun and then placed in an oven at 80 °C for 10 min. For Structure A, PEDOT:PSS was spin coated onto the substrate at 4000 rpm for 30 s, followed by annealing at 140 °C for 15 min. For Structure B, TFB solution (4 mg/ mL in chlorobenzene) and PVK (4 mg/mL in chlorobenzene) were sequentially spin coated onto the PEDOT:PSS layer at 4000 rpm for 45 s, followed by annealing at 150 °C for 20 min. For Structure C, the poly-TPD solution (10 mg/mL in chlorobenzene) was spin-coated onto the substrate at 4000 rpm for 45 s, followed by annealing at 150 °C for 20 min. Then a PVK layer was formed by spin coating the PVK solution (4 mg/mL in chlorobenzene) at 4000 rpm and annealing at 150 °C for 20 min. The quasi-2D perovskite precursor was deposited onto different HTLs (Structure A, B, and C) as mentioned above. The KBr-treated 3D perovskite precursor was deposited onto poly-TPD/PVK HTLs. The as-prepared substrates were then transferred to a thermal evaporator, and the chamber was pumped down to a base vacuum pressure of 2×10^{-6} Torr. TPBi (40 nm), LiF (1 nm), and Al elctrode (70 nm) were sequentially evaporated at deposition rates of 1, 0.3, and 2 Å/s, respectively. These devices were then encapsulated by UV epoxy (Ossila) and thin glass slides in a nitrogen-filled glovebox. All device tests were conducted in ambient conditions (21 $^{\circ}$ C, 40-50% humidity).

Current-Focusing Device Fabrication. For microsize current-focusing devices, a 150 nm ${\rm SiO_2}$ layer was first deposited onto the ITO-coated substrates by plasma enhanced chemical vapor deposition (PECVD) at 125 °C. The positive photoresist (AZ1512) was spin-coated onto substrates at 2000 rpm for 45 s and prebaked at 110 °C for 4 min. The photoresist was exposed for 3.5 s (Semiauto aligner, ABM) and then developed in AZ340 for 1 min. The microholes with different diameters were transferred to the ${\rm SiO_2}$ layer by plasma etching (ICP-Fluorine). The photoresist was then stripped by N-methyl-2-pyrrolidone (NMP) at 90 °C overnight.

For nanopatterned current-focusing devices, electron beam lithography was used to generate holes with a diameter of 100 nm. ZEP 520 resist (diluted in 1:1) was spin-coated onto the ITO-coated substrates at 2000 rpm for 60 s and baked at 180 °C for 5 min. The resist was exposed by an electron beam at a dose of 160 μ C/cm ² and then developed in amyl acetate for 2 min. The nanopatterned holes were transferred to the SiO₂ layer by plasma etching (ICP-Fluorine). The ZEP resist was finally stripped by NMP at 90 °C overnight. The

PeLEDs were then fabricated on substrates with current apertures with the same procedure as mentioned in the LED fabrication section.

Perovskite Film Characterization. The surface morphologies of perovskite films were analyzed by SEM (FEI, Siron) and AFM (Icon, Bruker). XRD patterns were recorded using Bruker D8 with a Cu K α radiation ($\lambda=1.54184$ Å). The PLQYs were measured using a CW laser ($\lambda=405$ nm), an integration sphere, and a spectrometer as reported elsewhere. 40 The quasi-2D and KBr-treated 3D perovskite films were deposited on clean glass substrates. The samples were clamped by a holder in an integration sphere, and the laser beam was focused onto samples with a convex lens. The focused beam size was determined by a CCD beam profiler (Thorlabs), and the power was measured by a silicon photodiode (Newport 818-UV). The PLQY was determined as the number of emitted photons to the number of absorbed photons.

For transient PL characterization, the samples were pumped by an ultrafast femtosecond Ti-sapphire laser with OPA ($\lambda=365$ nm, 50 fs). The pump power was adjusted by a variable attenuator wheel and detected by a hand-held detector (Coherent FieldMaster). The excitation laser beam profile was measured by a CCD beam profiler (Thorlabs, BC106N-VIS), and the beam diameter was determined by the $1/e^2$ cutoff of the Gaussian fit to the beam profile. The emitted PL from samples was collected by a pair of convex lenses and recorded by a streak camera with $\sim\!10$ ps time resolution. The IRF of the tr-PL setup was measured using glass in the same optical geometry as the sample measurements.

Performance Evaluation of Perovskite LEDs. The current density—voltage (J–V) characteristics were measured by a computer-controlled source meter (Keithley 6430). The voltage was swept from 1 to 9 V with a step voltage of 0.2 V. Simultaneously, front-face EL power output from the ITO side was measured by a calibrated silicon photodiode (Newport 818-SL) with a computer controlled optical meter (Newport 1830-C). The photodiode's active area (1 cm²) was well aligned with the emissive pixel. A Lambertian emission profile was assumed in calculating the total radiance. The EQE was calculated by dividing the number of emitted photons by the number of injected electrons. The EL spectra of PeLEDs were recorded by a fiber coupled spectrometer (Newport OSM 100). All device measurements were performed in a dark box under ambient conditions.

For pulsed current measurement, a current source (Newport LDP 3811) was used to provide current pulses (2 μs pulse width, 0.2% duty cycle, 1 kHz repetition rate). The emitted EL power was measured by a fast-response silicon photodiode (FDS1010, Thorlabs). The photodiode was connected to a custom-built large bandwidth transimpedance amplifier. The amplified signal was then sent to an oscilloscope for calculating the average EL power based on the responsivity of the photodiode.

Measurement of Operational Lifetime. The PeLEDs were driven by a constant current through a Keithley 6430. The initial luminance is set as $\sim 100 \text{ cd/m}^2$ by adjusting the drive current. The EL power was monitored by a silicon photodiode (Newport 818-SL), and the applied voltage was recorded by a Keithley 6430. The data was taken with an interval of 10 s.

ASSOCIATED CONTENT

Supporting Information

The Supporting Information is available free of charge at https://pubs.acs.org/doi/10.1021/acsnano.0c01817.

Additional notes on calculating the internal PLQY and electrically pumped lasing threshold and optical simulations of light outcoupling from PeLEDs; supplementary figures showing J–V characteristics of hole-only and electron-only devices, surface morphology characterization of perovskite films, the PLQY of PeLEDs under electrical biases, additional performance characterization of quasi-2D PeLEDs, PL comparison of KBr-treated 3D perovskite films, simulated PLQY of 3D perovskite films,

power distribution analysis in PeLEDs, performance characterization of microsize current-focusing devices, time-dependent EL response of PeLEDs under pulsed current operation, ASE characterization of KBr-treated 3D perovskite films, and dependence of electrically pumped lasing threshold (J × EQE) versus optically pumped ASE threshold; and tables showing detailed characteristics of devices in this work and performance comparison with other representative perovskite LEDs (PDF)

AUTHOR INFORMATION

Corresponding Author

Lih Y. Lin — Department of Electrical and Computer Engineering, University of Washington, Seattle, Washington 98195, United States; orcid.org/0000-0001-9748-5478; Email: lylin@uw.edu

Authors

Chen Zou — Department of Electrical and Computer Engineering, University of Washington, Seattle, Washington 98195, United States; orcid.org/0000-0001-9638-6363

Yun Liu — Department of Chemistry, University of Washington, Seattle, Washington 98195, United States; orcid.org/0000-0003-2312-5853

David S. Ginger — Department of Chemistry, University of Washington, Seattle, Washington 98195, United States

Complete contact information is available at: https://pubs.acs.org/10.1021/acsnano.0c01817

Author Contributions

C.Z. and L.Y.L conceived the project. C.Z. carried out all the experiments and data analysis. L.Y.L. supervised the project. Y.L. and D.S.G. contributed to the discussion and measurements on transient PL decay and PLQY. C.Z. drafted the manuscript, all authors provided inputs on data interpretation, discussion, manuscript revisions, and agreed to the final version.

Notes

The authors declare no competing financial interest.

ACKNOWLEDGMENTS

This work is supported by the National Science Foundation (Grant ECCS-1807397) and IP Group plc. Current-focusing device fabrication was conducted at the Washington Nanofabrication Facility, a National Nanotechnology Coordinated Infrastructure site at the University of Washington supported by the National Science Foundation (Grant NNCI-1542101). The study on carrier recombination dynamics was conducted at the Molecular Analysis Facility, a National Nanotechnology Coordinated Infrastructure site at the University of Washington supported in part by the National Science Foundation (Grant ECC-1542101), the University of Washington, the Molecular Engineering & Sciences Institute, the Clean Energy Institute, and the National Institutes of Health.

REFERENCES

(1) Lu, M.; Zhang, Y.; Wang, S.; Guo, J.; Yu, W. W.; Rogach, A. L. Metal Halide Perovskite Light-Emitting Devices: Promising Technology for Next-Generation Displays. Adv. Funct. Mater. 2019, 29, 1902008.

(2) Lin, K.; Xing, J.; Quan, L. N.; de Arquer, F. P. G.; Gong, X.; Lu, J.; Xie, L.; Zhao, W.; Zhang, D.; Yan, C.; Li, W.; Liu, X.; Lu, Y.;

- Kirman, J.; Sargent, E. H.; Xiong, Q.; Wei, Z. Perovskite Light-Emitting Diodes with External Quantum Efficiency Exceeding 20 Per Cent. Nature 2018, 562, 245—248
- Cent. Nature 2018, 562, 245–248.
 (3) Cao, Y.; Wang, N.; Tian, H.; Guo, J.; Wei, Y.; Chen, H.; Miao, Y.; Zou, W.; Pan, K.; He, Y.; Cao, H.; Ke, Y.; Xu, M.; Wang, Y.; Yang, M.; Du, K.; Fu, Z.; Kong, D.; Dai, D.; Jin, Y.; et al. Perovskite Light-Emitting Diodes Based on Spontaneously Formed Submicrometre-Scale Structures. Nature 2018, 562, 249–253.
- (4) Xing, J.; Zhao, Y.; Askerka, M.; Quan, L. N.; Gong, X.; Zhao, W.; Zhao, J.; Tan, H.; Long, G.; Gao, L.; Yang, Z.; Voznyy, O.; Tang, J.; Lu, Z. H.; Xiong, Q.; Sargent, E. H. Color-Stable Highly Luminescent Sky-Blue Perovskite Light-Emitting Diodes. Nat. Commun. 2018, 9, 3541
- (5) Ban, M.; Zou, Y.; Rivett, J. P. H.; Yang, Y.; Thomas, T. H.; Tan, Y.; Song, T.; Gao, X.; Credgington, D.; Deschler, F.; Sirringhaus, H.; Sun, B. Solution-Processed Perovskite Light Emitting Diodes with Efficiency Exceeding 15% through Additive-Controlled Nanostructure Tailoring. Nat. Commun. 2018, 9, 3892.
- (6) Yang, X.; Zhang, X.; Deng, J.; Chu, Z.; Jiang, Q.; Meng, J.; Wang, P.; Zhang, L.; Yin, Z.; You, J. Efficient Green Light-Emitting Diodes Based on Quasi-Two-Dimensional Composition and Phase Engineered Perovskite with Surface Passivation. Nat. Commun. 2018, 9, 570.
- (7) Li, Z.; Chen, Z.; Yang, Y.; Xue, Q.; Yip, H. L.; Cao, Y. Modulation of Recombination Zone Position for Quasi-Two-Dimensional Blue Perovskite Light-Emitting Diodes with Efficiency Exceeding 5%. Nat. Commun. 2019, 10, 1027.
- (8) Shang, Y.; Li, G.; Liu, W.; Ning, Z. Quasi-2D Inorganic CsPbBr3 Perovskite for Efficient and Stable Light-Emitting Diodes. Adv. Funct. Mater. 2018, 28, 1801193.
- (9) Zhao, B.; Bai, S.; Kim, V.; Lamboll, R.; Shivanna, R.; Auras, F.; Richter, J. M.; Yang, L.; Dai, L.; Alsari, M.; She, X.-J.; Liang, L.; Zhang, J.; Lilliu, S.; Gao, P.; Snaith, H. J.; Wang, J.; Greenham, N. C.; Friend, R. H.; Di, D. High-Efficiency Perovskite-Polymer Bulk Heterostructure Light-Emitting Diodes. Nat. Photonics 2018, 12, 783–789
- (10) Han, B.; Cai, B.; Shan, Q.; Song, J.; Li, J.; Zhang, F.; Chen, J.; Fang, T.; Ji, Q.; Xu, X.; Zeng, H. Stable, Efficient Red Perovskite Light-Emitting Diodes by (α, δ) -CsPbI $_3$ Phase Engineering. Adv. Funct. Mater. 2018, 28, 1804285.
- (11) Xu, W.; Hu, Q.; Bai, S.; Bao, C.; Miao, Y.; Yuan, Z.; Borzda, T.; Barker, A. J.; Tyukalova, E.; Hu, Z.; et al. Rational Molecular Passivation for High-Performance Perovskite Light-Emitting Diodes. Nat. Photonics 2019, 13, 418–424.
- (12) Shen, Y.; Cheng, L. P.; Li, Y. Q.; Li, W.; Chen, J. D.; Lee, S. T.; Tang, J. X. Perovskite Light-Emitting Diodes: High-Efficiency Perovskite Light-Emitting Diodes with Synergetic Outcoupling Enhancement. Adv. Mater. 2019, 31, 1970174.
- (13) Huang, C.-Y.; Zou, C.; Mao, C.; Corp, K. L.; Yao, Y.-C.; Lee, Y.-J.; Schlenker, C. W.; Jen, A. K. Y.; Lin, L. Y. CsPbBr₃ Perovskite Quantum Dot Vertical Cavity Lasers with Low Threshold and High Stability. ACS Photonics 2017, 4, 2281–2289.
- (14) Jia, Y.; Kerner, R. A.; Grede, A. J.; Rand, B. P.; Giebink, N. C. Continuous-Wave Lasing in an Organic-Inorganic Lead Halide Perovskite Semiconductor. Nat. Photonics 2017, 11, 784–788.
- (15) Leyden, M. R.; Terakawa, S.; Matsushima, T.; Ruan, S.; Goushi, K.; Auffray, M.; Sandanayaka, A. S. D.; Qin, C.; Bencheikh, F.; Adachi, C. Distributed Feedback Lasers and Light-Emitting Diodes Using 1-Naphthylmethylamnonium Low-Dimensional Perovskite. ACS Photonics 2019, 6, 460–466.
- (16) Fakharuddin, A.; Qiu, W.; Croes, G.; Devizis, A.; Gegevicius, R.; Vakhnin, A.; Rolin, C.; Genoe, J.; Gehlhaar, R.; Kadashchuk, A.; Gulbinas, V.; Heremans, P. Reduced Efficiency Roll-Off and Improved Stability of Mixed 2D/3D Perovskite Light Emitting Diodes by Balancing Charge Injection. Adv. Funct. Mater. 2019, 29, 1904101.
- (17) Murawski, C.; Leo, K.; Gather, M. C. Efficiency Roll-Off in Organic Light-Emitting Diodes. Adv. Mater. 2013, 25, 6801–6827.

- (18) Shirasaki, Y.; Supran, G. J.; Tisdale, W. A.; Bulovic, V. Origin of Efficiency Roll-Off in Colloidal Quantum-Dot Light-Emitting Diodes. Phys. Rev. Lett. 2013, 110, 217403.
- (19) Sun, Y.; Su, Q.; Zhang, H.; Wang, F.; Zhang, S.; Chen, S. Investigation on Thermally Induced Efficiency Roll-Off: Toward Efficient and Ultrabright Quantum-Dot Light-Emitting Diodes. ACS Nano 2019, 13, 11433–11442.
- (20) Zou, W.; Li, R.; Zhang, S.; Liu, Y.; Wang, N.; Cao, Y.; Miao, Y.; Xu, M.; Guo, Q.; Di, D.; Zhang, L.; Yi, C.; Gao, F.; Friend, R. H.; Wang, J.; Huang, W. Minimising Efficiency Roll-Off in High-Brightness Perovskite Light-Emitting Diodes. Nat. Commun. 2018, 9, 608.
- (21) Yang, M.; Wang, N.; Zhang, S.; Zou, W.; He, Y.; Wei, Y.; Xu, M.; Wang, J.; Huang, W. Reduced Efficiency Roll-Off and Enhanced Stability in Perovskite Light-Emitting Diodes with Multiple Quantum Wells. J. Phys. Chem. Lett. 2018, 9, 2038–2042.
- (22) Sim, K.; Jun, T.; Bang, J.; Kamioka, H.; Kim, J.; Hiramatsu, H.; Hosono, H. Performance Boosting Strategy for Perovskite Light-Emitting Diodes. Appl. Phys. Rev. 2019, 6, 031402.
- (23) Shen, H.; Gao, Q.; Zhang, Y.; Lin, Y.; Lin, Q.; Li, Z.; Chen, L.; Zeng, Z.; Li, X.; Jia, Y.; Wang, S.; Du, Z.; Li, L. S.; Zhang, Z. Visible Quantum Dot Light-Emitting Diodes with Simultaneous High Brightness and Efficiency, Nat. Photonics 2019, 13, 192–197
- Brightness and Efficiency. Nat. Photonics 2019, 13, 192–197. (24) Brenner, P.; Bar-On, O.; Jakoby, M.; Allegro, I.; Richards, B. S.; Paetzold, U. W.; Howard, I. A.; Scheuer, J.; Lemmer, U. Continuous Wave Amplified Spontaneous Emission in Phase-Stable Lead Halide Perovskites. Nat. Commun. 2019, 10, 988.
- (25) Nakanotani, H.; Oyamada, T.; Kawamura, Y.; Sasabe, H.; Adachi, C. Injection and Transport of High Current Density over 1000 A/cm² in Organic Light Emitting Diodes under Pulse Excitation. Jpn. J. Appl. Phys. 2005, 44, 3659–3662.
- (26) Setoguchi, Y.; Adachi, C. Suppression of Roll-Off Characteristics of Electroluminescence at High Current Densities in Organic Light Emitting Diodes by Introducing Reduced Carrier Injection Barriers. J. Appl. Phys. 2010, 108, 064516.
- (27) Giuri, A.; Yuan, Z.; Miao, Y.; Wang, J.; Gao, F.; Sestu, N.; Saba, M.; Bongiovanni, G.; Colella, S.; Esposito Corcione, C.; Gigli, G.; Listorti, A.; Rizzo, A. Ultra-Bright Near-Infrared Perovskite Light-Emitting Diodes with Reduced Efficiency Roll-off. Sci. Rep. 2018, 8, 15496.
- (28) Kim, H.; Zhao, L.; Price, J. S.; Grede, A. J.; Roh, K.; Brigeman, A. N.; Lopez, M.; Rand, B. P.; Giebink, N. C. Hybrid Perovskite Light Emitting Diodes under Intense Electrical Excitation. Nat. Commun. 2018, 9, 4893.
- (29) Wang, Y.; Teng, Y.; Lu, P.; Shen, X.; Jia, P.; Lu, M.; Shi, Z.; Dong, B.; Yu, W. W.; Zhang, Y. Low Roll-Off Perovskite Quantum Dot Light-Emitting Diodes Achieved by Augmenting Hole Mobility. Adv. Funct. Mater. 2020, 1910140.
- (30) Byun, J.; Cho, H.; Wolf, C.; Jang, M.; Sadhanala, A.; Friend, R. H.; Yang, H.; Lee, T. W. Efficient Visible Quasi-2D Perovskite Light-Emitting Diodes. Adv. Mater. 2016, 28, 7515–20.
- (31) Žou, Y.; Ban, M.; Yang, Y.; Bai, S.; Wu, C.; Han, Y.; Wu, T.; Tan, Y.; Huang, Q.; Gao, X.; Song, T.; Zhang, Q.; Sun, B. Boosting Perovskite Light-Emitting Diode Performance via Tailoring Interfacial Contact. ACS Appl. Mater. Interfaces 2018, 10, 24320–24326.
- (32) Liu, Y.; Wu, T.; Liu, Y.; Song, T.; Sun, B. Suppression of Non-Radiative Recombination toward High Efficiency Perovskite Light-Emitting Diodes. APL Mater. 2019, 7, 021102.
- (33) Liu, Y.; Cui, J.; Du, K.; Tian, H.; He, Z.; Zhou, Q.; Yang, Z.; Deng, Y.; Chen, D.; Zuo, X.; Ren, Y.; Wang, L.; Zhu, H.; Zhao, B.; Di, D.; Wang, J.; Friend, R. H.; Jin, Y. Efficient Blue Light-Emitting Diodes Based on Quantum-Confined Bromide Perovskite Nanostructures. Nat. Photonics 2019, 13, 760–764.

 (34) Straus, D. B.; Kagan, C. R. Electrons, Excitons, and Phonons in
- (34) Straus, D. B.; Kagan, C. R. Electrons, Excitons, and Phonons in Two-Dimensional Hybrid Perovskites: Connecting Structural, Optical, and Electronic Properties. J. Phys. Chem. Lett. 2018, 9, 1434–1447.

- (35) Kirkwood, N.; Singh, B.; Mulvaney, P. Enhancing Quantum Dot LED Efficiency by Tuning Electron Mobility in the ZnO Electron Transport Layer. Adv. Mater. Interfaces 2016, 3, 1600868.
- (36) Straus, D. B.; Iotov, N.; Gau, M. R.; Zhao, Q.; Carroll, P. J.; Kagan, C. R. Longer Cations Increase Energetic Disorder in Excitonic 2D Hybrid Perovskites. J. Phys. Chem. Lett. 2019, 10, 1198–1205.
- (37) Xing, G.; Wu, B.; Wu, X.; Li, M.; Du, B.; Wei, Q.; Guo, J.; Yeow, E. K.; Sum, T. C.; Huang, W. Transcending the Slow Bimolecular Recombination in Lead-Halide Perovskites for Electroluminescence. Nat. Commun. 2017, 8, 14558.
- (38) Milot, R. L.; Eperon, G. E.; Green, T.; Snaith, H. J.; Johnston, M. B.; Herz, L. M. Radiative Monomolecular Recombination Boosts Amplified Spontaneous Emission in HC(NH2)₂SnI₃ Perovskite Films. J. Phys. Chem. Lett. 2016, 7, 4178–4184.
- (39) Richter, J. M.; Abdi-Jalebi, M.; Sadhanala, A.; Tabachnyk, M.; Rivett, J. P. H.; Pazos-Outon, L. M.; Godel, K. C.; Price, M.; Deschler, F.; Friend, R. H. Enhancing Photoluminescence Yields in Lead Halide Perovskites by Photon Recycling and Light Out-Coupling. Nat. Commun. 2016, 7, 13941.
- (40) DeQuilettes, D. W.; Koch, S.; Burke, S.; Paranji, R. K.; Shropshire, A. J.; Ziffer, M. E.; Ginger, D. S. Photoluminescence Lifetimes Exceeding 8 µs and Quantum Yields Exceeding 30% in Hybrid Perovskite Thin Films by Ligand Passivation. ACS Energy Lett. 2016, 1, 438–444.
- (41) Braly, I. L.; DeQuilettes, D. W.; Pazos-Outon, L. M.; Burke, S.; Ziffer, M. E.; Ginger, D. S.; Hillhouse, H. W. Hybrid Perovskite Films Approaching the Radiative Limit with over 90% Photoluminescence Quantum Efficiency. Nat. Photonics 2018, 12, 355–361.
- (42) Abdi-Jalebi, M.; Andaji-Garmaroudi, Z.; Cacovich, S.; Stavrakas, C.; Philippe, B.; Richter, J. M.; Alsari, M.; Booker, E. P.; Hutter, E. M.; Pearson, A. J.; Lilliu, S.; Savenije, T. J.; Rensmo, H.; Divitini, G.; Ducati, C.; Friend, R. H.; Stranks, S. D. Maximizing and Stabilizing Luminescence from Halide Perovskites with Potassium Passivation. Nature 2018, 555, 497–501.
- (43) Cho, H.; Kim, Y. H.; Wolf, C.; Lee, H. D.; Lee, T. W. Improving the Stability of Metal Halide Perovskite Materials and Light-Emitting Diodes. Adv. Mater. 2018, 30, 1704587.
- (44) Lee, H.; Ko, D.; Lee, C. Direct Evidence of Ion-Migration-Induced Degradation of Ultrabright Perovskite Light-Emitting Diodes. ACS Appl. Mater. Interfaces 2019, 11, 11667–11673.
- Diodes. ACS Appl. Mater. Interfaces 2019, 11, 11667–11673. (45) Zou, C.; Huang, C. Y.; Sanehira, E. M.; Luther, J. M.; Lin, L. Y. Highly Stable Cesium Lead Iodide Perovskite Quantum Dot Light-Emitting Diodes. Nanotechnology 2017, 28, 455201.
- (46) Chen, Z.; Li, Z.; Zhang, C.; Jiang, X. F.; Chen, D.; Xue, Q.; Liu, M.; Su, S.; Yip, H. L.; Cao, Y. Recombination Dynamics Study on Nanostructured Perovskite Light-Emitting Devices. Adv. Mater. 2018, 30, 1801370
- (47) deQuilettes, D. W.; Frohna, K.; Emin, D.; Kirchartz, T.; Bulovic, V.; Ginger, D. S.; Stranks, S. D. Charge-Carrier Recombination in Halide Perovskites: Focus Review. Chem. Rev. 2019, 119, 11007–11019.
- (48) Li, J.; Yuan, X.; Jing, P.; Li, J.; Wei, M.; Hua, J.; Zhao, J.; Tian, L. Temperature-Dependent Photoluminescence of Inorganic Perovskite Nanocrystal Films. RSC Adv. 2016. 6, 78311–78316.
- skite Nanocrystal Films. RSC Adv. 2016, 6, 78311–78316. (49) Koh, T.-W.; Spechler, J. A.; Lee, K. M.; Arnold, C. B.; Rand, B. P. Enhanced Outcoupling in Organic Light-Emitting Diodes via a High-Index Contrast Scattering Layer. ACS Photonics 2015, 2, 1366–1372.
- (50) Lim, J.; Park, Y. S.; Klimov, V. I. Optical Gain in Colloidal Quantum Dots Achieved with Direct-Current Electrical Pumping. Nat. Mater. 2018, 17, 42–49.
- (51) Matsushima, T.; Sasabe, H.; Adachi, C. Carrier Injection and Transport Characteristics of Copper Phthalocyanine Thin Films under Low to Extremely High Current Densities. Appl. Phys. Lett. 2006, 88, 033508.
- (52) Xu, M.; Peng, Q.; Zou, W.; Gu, L.; Xu, L.; Cheng, L.; He, Y.; Yang, M.; Wang, N.; Huang, W.; Wang, J. A Transient-Electroluminescence Study on Perovskite Light-Emitting Diodes. Appl. Phys. Lett. 2019, 115, 041102.

- (53) Hayashi, K.; Nakanotani, H.; Inoue, M.; Yoshida, K.; Mikhnenko, O.; Nguyen, T.-Q.; Adachi, C. Suppression of Roll-Off Characteristics of Organic Light-Emitting Diodes by Narrowing Current Injection/Transport Area to 50nm. Appl. Phys. Lett. 2015, 106, 093301.
- (54) Kuwae, H.; Nitta, A.; Yoshida, K.; Kasahara, T.; Matsushima, T.; Inoue, M.; Shoji, S.; Mizuno, J.; Adachi, C. Suppression of External Quantum Efficiency Roll-Off of Nanopatterned Organic-Light Emitting Diodes at High Current Densities. J. Appl. Phys. 2015, 118, 155501.